

6

Application of Computational Aerodynamics for Blades Shape Optimization

6.1 Problem Statement

The rapid development of computational aerodynamics methods not only puts on the agenda introduction of the spatial calculations into the turbines design practice, but also raises the need to develop the blades shape and other turbine flow path elements optimization methods taking into account 3D flow [24].

Formulations of the blades spatial optimization problems, which essentially cannot be solved by using one-dimensional and two-dimensional models, for minimization of the secondary flows losses, arising at the tip and the hub of the blades, are of the greatest interest [35].

Analyzing the results of the research, three main reasons for formation of the secondary flows in the turbine cascades could be singled out:

1) *Turning of the flow*. In channels with flow turning (including the turbine cascades) the transverse gradient of pressure arises, under influence of which whirlwind is forming at the ends of the channel.

2) *Interaction of the boundary layer, accumulated on the end wall in front of the blade* with the leading edge of the blade. For this reason, a horseshoe-shaped whirlwind is formed, which is then divided into two parts on both sides of the blade.

3) *Vortex wedge*. In almost every corner areas, which are generated between vortical structures and walls of turbine channel cascade, the forming or dissipating of corner vortexes may take place. Some from them are there constantly, some are dissipating depending from the flow parameters and the type of the wedge.

To the most important causes inducing the secondary losses, relate the following factors:

- 1) natural accumulation of the boundary layer on end wall at the entrance till the lines of detachment;
- 2) braked the detachable bubble in the field of entrance edge between two lines of the detachment;
- 3) increasing the new boundary layer after the line of detachment;
- 4) losses in the corners between the high and low pressure sides and end wall (the most significant losses are situated in the corner between the low pressure side and end wall);
- 5) influence of tangential stresses along the $3D$ lines of detachment;
- 6) loss caused by tangential stresses between the channel vortex and the low pressure side of the blade, as well as the process of mixing of the crosscut flow with the flow in the channel along with a three-dimensional line of detachment;
- 7) dissipation of all vortexes and complete mixing of heterogeneous flow field at the cascade exit.

Such a complex character of the influence of secondary flows on cascade losses requires investigation of means of their minimization through appropriate selection of the blades shape in the end zones. Management of the end phenomena may be implemented by changing the shape of the profile along the height of the blades, using the complex tangential lean, profiling of the form of the flow path, utilization of the additional aerodynamic elements in channels between the blades.

The most evident way to control the flow nearby the ends of the blades is a lean. The simple problem statement of lean optimization involves parameterization of the blades shape by means of deformation of the stacking line in accordance with the chosen law. Selection of the deformation parameters, using one of the methods of direct search, leads to the definition of a profile

shape that ensures minimum integral losses in the cascade. Despite its apparent simplicity, this approach requires overcoming several problems associated with the efficiency of the solving of the putted task, in particular: rapid and reliable ways of building a parameterized blades and corresponding with them calculation grids in the blade passages; development of the mechanisms of data exchange with *CFD*-solvers; elaboration of recommendations for solver settings, providing sufficient accuracy and speed of calculations; the choice of optimization method, usable for solving the problems with difficult computable objective functions and with various kinds of restrictions.

6.2 Representation of Blades Geometry

6.2.1 File Formats for Blades Storage

Sources of geometric information related to turbines blades are quite varied.

These can be drawings in the paper or electronic form, the results of measurement of coordinates of the dots multitude, using mechanical or laser devices, coordinates of cross sections by flat or conical surfaces.

When the surface of the blade is represented by sets of dots its conical (cylindrical for axial machines) cross sections, it is assumed that the program, taking this information, will build the splines on cross sections and then will stretch the spline on surface. In this sense, this description is procedural.

In particular, the BladeGen preprocessor (*Ansys CFX*) offers two format of procedural form of the blades storing – *RTZT* and *CURVE*. Because the information in the *CURVE* file is not enough for permanent storage of data of the blade wheel, we have developed its extension – *CUR* format. It additionally includes the number of blades in the crown, the number of the cross sections and the number of the profile sectors in the cross sections, the number of dots in the sectors, etc.

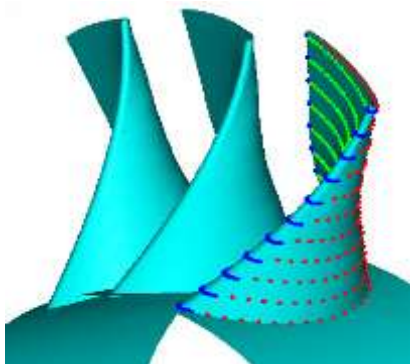


Figure 6.1 Fragment of the blade wheel stored in the CUR format (4 sectors on the profile).

The number of sectors on the contour of the cross section can be 1, 2 or 4. In the first case, the surface of the blade is formed by one spline. Accordingly, in the second and third cases, the blades is formed by two (suction and pressure sides) or four (suction side, leading edge, pressure side and trailing edge) spline segments.

The order and type of splines (for example, interpolation or approximation) are not stored in a file, because these options are implementation-dependent. They must be specified in the reading procedure. A fragment of the blade wheel, described using the CUR format with four sectors in each of the five initial cross sections of the blade, is shown at Fig. 6.1. The cross sections, shown at Fig. 6.1, came out as a result of spline-approximation of original dots (dots on the sites have different colors).

6.2.2 Stacking

The process of drawing up the blades from known cross sections (flat or cylindrical) is called *stacking*. To do this, specific point of each cross section, which coincides with the stacking line of this cross section, must be selected. Often, for convenience, the centers of the edges or the centers of gravity of the cross sections are chosen as stacking points (Fig. 6.2). In general, this selection can significantly change the shape of the blades.

Any deviation of the stacking line from radial location will be named *lean*. With a simple lean stacking line remains straight and is characterized by a single parameter –the angle of incline. When we have a complex lean it can take

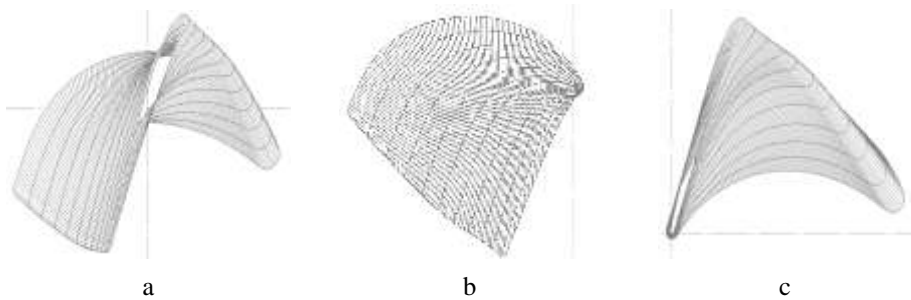


Figure 6.2 *The simplest methods of the blade forming: a – radial center of gravity; b – radial center of inlet edge; c – radial center of outlet edge any form. There is distinguishing among axial and tangential lean.*

For easy use, it makes sense to limit parameterization of stacking line by Bezier curves.

6.2.3 Forming the Lateral Surfaces of the Blades

The surface of the blade is described by the parametric functions-interpolation or approximation *B*-splines based on two parameters: *u*-along the contour of each cross section and *v*-along the direction of stacking. Interpolation spline passes exactly through all dots of cross-section of the blade, and approximation spline – in accordance with supporting polygon, which is build using the dots of cross section or by least squares method [36]. All dots of the surface can be found, when *u* and *v* parameters taking the values from 0 to 1. In some cases, it is required to allow extrapolation towards the staking and then the *v* parameter may become a bit less than 0 or greater than 1.

The blade can be described either by one surface or by several. In our implementation (as already noted) 2 or 4 surfaces, that can be useful for some applications, in particular, when constructing grids, are allowed. Since there is no

joining on surface boundary, the junction's error could be managed only changing the spline order along u and v directions. It is usually within the range 2...5.

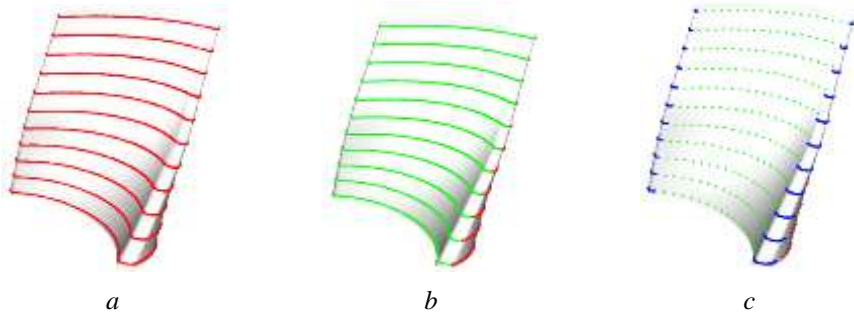


Figure 6.3 The blade surface formation, using one (a), two (b) and four (c) surfaces.

6.2.4 Three-Dimensional the Turbine Blade Parametric Model

One of the key elements of the 3D aerodynamic optimization of the turbine cascades algorithm is the turbine blade model parameterization, which consists in the possibility of changing blade shape (curvature) by variation of the limited number of numeric parameters that describes the stacking line.

The Bezier curve of 3-d (method 1) and 4-th order (method 2) it seems convenient to use as the binding line. The second method allows creating a stacking line with practically straight-line the middle segment. (Fig. 6.4, 6.5). The number of independent variables in both cases can be reduced to two (Y_h and Y_s).

Parametric model of turbine blades must provide an opportunity to check the mass flow through the cascade. This requires incorporation in the model parameter, which allows controlling the mass flow during optimization. Most eventually the last gives the possibility to ensure equality of the mass flow between initial and optimized cascades with the same flow parameters before and after cascades. The changing of stagger angle of the blade, relative to the original, can be taken as such parameter.

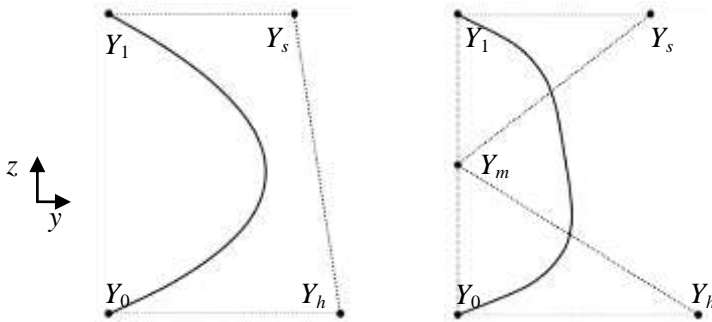


Figure 6.4 Bezier curves of 3-rd and 4-th order.

In addition to complex lean, the simple lean was implemented in methodical aim, which consists in turning of the turbine blades profiles relatively of the axis of rotation of the turbine on the specified angle. In general, developed parametric model of turbine blade allows producing its curvature in the circumferential (tangential) direction as well as in axial direction, simultaneously or separately.

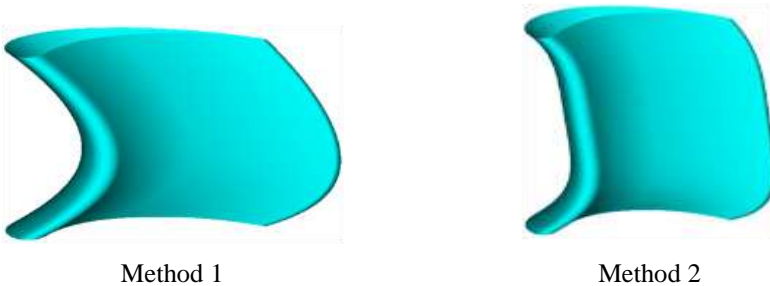


Figure 6.5 Shapes of the blades with complex lean.

6.2.5 The Grids Construction

As it is known, the results of the *CFD* calculations may depend on the type of calculation grids. One of the tasks, needing to be addressed, is to build up a three-dimensional parametric calculation grids, satisfying the form of parameterized blades.

Fast and reliable building of the parametric calculation grids is an integral part of the optimization studies as it implies the calculation of a large number of variants of the geometry of the turbine cascade. Since the developed algorithm of optimization should not be tied up with solitary *CFD*-solver, a specialized grids builder has been developed.

We will describe in details the work with *H*-grids, which represent a convenient compromise between complexity of the grids creation and quality of the obtained solutions when flows computation in turbomachine cascades occur. *H*-grid topologically is equivalent to the cube. Therefore, a data structure is simple enough for description. It intentionally is made redundant to accelerate frequently meeting operations. This, of course, slightly reduces the maximum size of the grid when a limited amount of RAM available to the computer, but it is not critical to the solving problem.

The structured calculation grid for channel between the blades is obtained because of deformation in the direction of each of the coordinate axes of a rectangular parallelepiped (in space) or rectangle (flat case).

Inter-blade channel is formed by concave and convex sides of the two adjacent blades (or profiles in the planar case). For selecting the high pressure and low pressure sides of the blade, the blade is made up by two splines, connecting in the points of minimum and maximum x -coordinate sections. Parametric lines $v = \text{const}$ of these splines give the calculated coordinates of D sections of the grid in the radial direction. Next inter-blade channels are supplemented by input and output sections of the specified length, representing segments of the rings (for circumferential blade cascade) or parallelepiped (for flat cascade). The resulting area in each section is split up to cells of grids in the direction of x -coordinates dimension L . On the inlet and outlet sections is usually taken by $L/4$ cells. Other cells are located on the profile and coordinates

of the nodes are calculated by interpolation spline via dots of the splines of the high and low pressure sides.

Finally, channels are split on H sections along the directions $x = \text{const}$, that completes the structured grid formation. In the process of grid building a primitives numbering (nodes, edges, verges, and cells), topological ties formation and geometrical data calculation are made. All information is entered into a data structure.

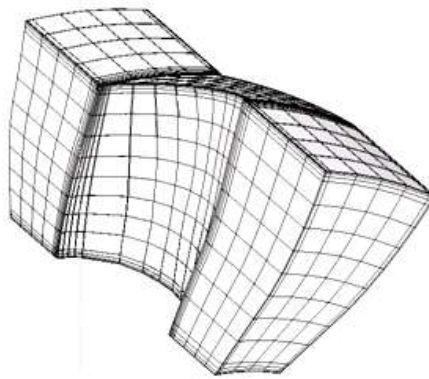


Figure 6.6 *The spatial H-grid of inter-blade channel $32 \times 8 \times 16$ with thickening in three directions.*

As such, the calculated grids are not yet suitable for conducting reliable calculations of viscous flows in the blades cascades. They should be improved in order to fit the peculiarities of the flow near the walls of the channel.

Thickening structured grid is performed independently for each of the coordinate directions. Law of deformation of the grid can be different and should reflect the physical characteristics of the flow in the area of thickening. For example, near the wall polynomial law for changing the grid can be used, which corresponds to the rate of changing the velocity in the boundary layer. In the area of input and output edges the deformation may be exponential in nature that is less aggressive. In either case, a number of parameters controlling the

thickening as for the rate of deformation as well as the ratio of the sizes of areas of the channel subject to or not to distortion should be entered.

In general three-dimensional case, the grid, suitable for calculations of viscous flows, is presented at Fig. 6.6.

6.2.6 File Format for Grids Storage

The diversity of formats creates some difficulty in reading these files by different *CFD*-applications. *CGNS*-standard for *CFD* calculations data storage is positioned as a "common, portable and extensible". Software implementation of the standard is an open, cross-platform and well documented that, in principle, precludes differences of various applications.

Data in *CGNS* format are stored in binary form and access to it is implemented through a set of functions for reading, writing, and modifying of the contents of the files which can be called from application in different programming languages. In general case *CGNS* file can contain data which is associated with viscous compressible fluid flow, but suitable for solutions of the Euler equations and potential flows.

The standard includes the following data types: structured, unstructured hybrid grids; data of the *CFD* calculations; information on the sub-grids docking or overlapping; boundary conditions; descriptions of equations of state, turbulence models etc.; nonstationary solutions, including deformation of calculation grids in time; dimension of variables; variables reference points; history of calculations; user's and other data.

For the purpose of specific tasks solution there is no need to implement in full all the functionality, supported by the *CGNS* (this is not currently doing even such advanced products like *CFX*). It is enough, for example, organize saving of the structured grids and setting of the boundary conditions, satisfying the terms of the calculation task. This significantly speeds up the preparation of

data for *CFD* calculations. Analysis of output information, perhaps, you might need to implement by means of post-processors of used packages, since not all of them conserve the results of calculations in *CGNS* format.

6.3 *CFD* Tools

For realization of the optimization algorithm, using *CFD*-calculations, it is necessary to choose the right program product.

Well known program complex *ANSYS CFX* includes in it pre-processor, post-processor and the solver.

ANSYS CFX Solver has the following characteristics:

- *numerical methods*: finite volume discretization of equations; solution of the complete three-dimensional unsteady Navier-Stokes equations; difference schemes of 1-2order; the joint solution of the equations of conservation of mass and moment; algebraic multigrid method for solving the linearized equations; support of the elements of various types – hexahedrons, prisms, pyramids, tetrahedrons; adaptive thickening of grids; movable and changing grids;
- *model of turbulence*: algebraic model; model $k-\varepsilon$; $k-\omega$ model; model SST; Reynolds stress model; method of large vortices LES; method of not attached vortex DES.

The program complex *ANSYS CFX* has the following level of support for *CGNS* format:

- preprocessor supports only reading of grids and names of edges of the computational domain;
- solver does not support the reading of *CGNS* files, but allows to convert the results of calculation in *CGNS* format;

- post-processor supports the reading of the calculation results.

The preprocessor is used for entering the *CGNS* files and setting the boundary conditions for each variant of blades geometry, even when the boundary conditions and calculation parameters are identical.

Calculation in *ANSYS CFX-Solver* is made then.

Processing and the analysis of results takes place in postprocessor, using macros that are intended for determination of the values, required in the process of optimization.

6.4 Algorithm of Spatial Aerodynamic Optimization of the Blade Cascades of Axial Turbines

The proposed method of optimization of the cascades is based on the joint usage of the formal macromodeling and $LP\tau$ search and includes the following steps [37]:

The plan of computing experiment is created [1, 2]. In the given range of variable parameters, defining a stacking line, the points, in which computations will be carried out, are determined.

The blades matching of the plan points parameters are constructed and computation domain and grids are generated.

Values of objective function for each combination of parameters are determined. For this purpose *CFD* computation and post-processing of results are carried out.

Coefficients of a full square-law polynomial type (1.2) or (1.12) of objective function and restriction function in the set range of varied parameters are determined. Using $LP\tau$ search the minimum of value losses in the cascade

$\zeta(Y_h, Y_s, \Delta\beta_s)$ is determined, under condition that the mass flow through it satisfies the condition $|G(Y_h, Y_s, \Delta\beta_s) - G_{org}| < \varepsilon$.

The scope of varied parameters has been changed:

- a) if the minimum of the objective function appears on the border of the range of variation parameters, the last is displaced aside of this boundary;
- b) if the minimum of the objective function are inside of the range, but macromodel is not sufficiently precise, the range decreases;
- c) if the minimum function falls within the range and macro-model is accurate enough, checking *CFD*-calculation is carried out and if its results with sufficient accuracy coincide with optimization results on macromodel, optimization is completed, otherwise the range decreases. Repeat pt. 1–4.

6.5 The Impact of Simple Tangential Lean on the Flow Through the Turbine Circumferential Cascade

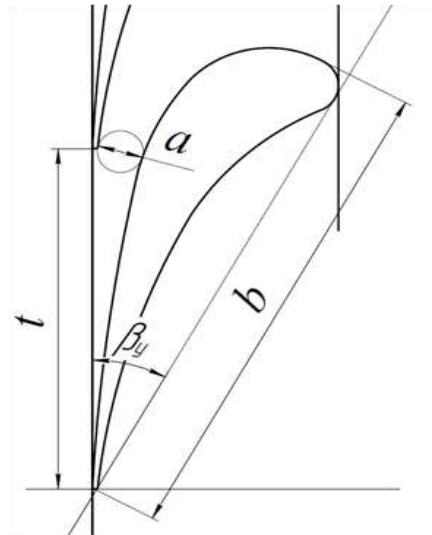


Figure 6.7 Researched blade profile TC-1A.

It is known that the lean along the flow leads to increasing secondary flow losses on the periphery and to reducing them at the root. Lean against the stream leads, correspondingly, to the opposite result.

The lean to the opposite flow direction allows to alter the distribution of flow parameters along height, so that the leakages in the axial gap is reduced on the periphery, that positively affects stage efficiency.

As an object of research the circumferential guide blade cascade was chosen with the profiles TC-1A (Fig. 6.7) with the following parameters:

$$b = 0.26 \text{ m}; \quad \bar{t}_h = 0.715; \quad \bar{t}_t = 0.864; \quad \beta_s = 61^\circ; \quad l/b = 0.49$$

and centering on the input edge.

Boundary conditions:

- inlet: $P_0^2 = 102240 \text{ Pa}; T_0^* = 373.15 \text{ K};$
- the degree of turbulence 1%;
- outlet: $P_2 = 81861 \text{ Pa};$
- the blade and the ends of the channel: impermeable wall with condition of sticking the flow;
- working medium: air.

In the investigated guide blade cascade boundary conditions correspond to subsonic flow with Reynolds number at outlet equals $2 \cdot 10^6$.

Fig. 6.8–6.10 shows the results of calculations with lean angles $\gamma = -30; -20; -10; 0; 10; 20; 30^\circ$ (negative lean means the lean against the direction of the flow and positive – the lean in the direction of the stream).

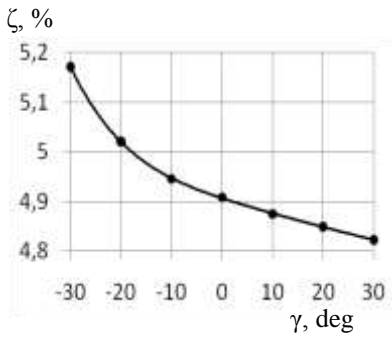


Figure 6.8 Change of the integral losses coefficient from lean.

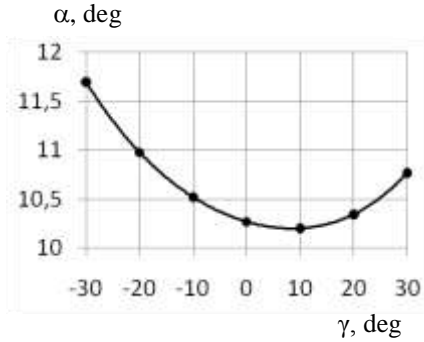


Figure 6.9 Change of the integral actual outlet flow angle from lean.

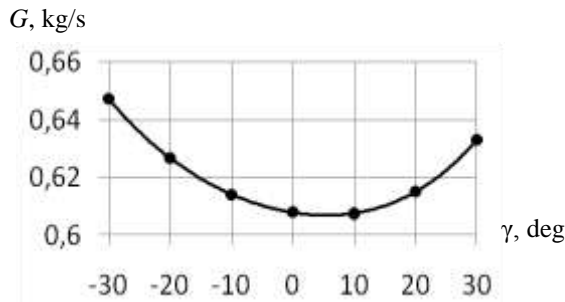


Figure 6.10 Change of mass flow rate from lean.

Obviously, that the total losses are increasing when there is negative lean and decreasing with the positive lean. Exit angle of the flow and the mass flow rate is increasing as with positive and with negative lean.

The mode of the changing of the actual outlet flow angle is shown at Fig. 6.11. Positive lean leads to an increase in the actual outlet flow angle near the root and decrease on the periphery; negative lean brings to the opposite effect. Given the nature of allocation of the losses along height of the blade as a lean result (Fig. 6.12), possible to say that an increase of the outlet flow angle leads to the secondary losses reducing.

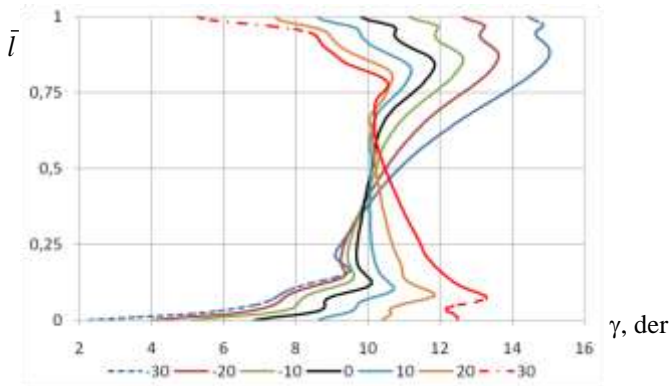


Figure 6.11 Distribution of actual outlet flow angle along the blade height.

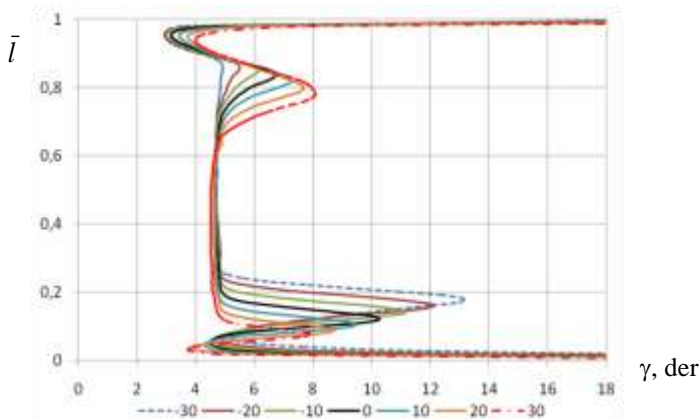


Figure 6.12 Distribution of losses coefficient along the height behind cascade with different blades leans.

An increase of the mass flow rate, as with a positive and with a negative lean occurs due to an increase in the integral actual outlet flow angle. In addition, with positive lean into increase of the mass flow rate also contributes reducing the integral losses and, accordingly, with a negative lean increasing of the losses slightly brings down increasing the mass flow rate, which takes place as a result of increase of the outlet flow angle.

The reasons for this significant changing of flow parameters with lean of the blades may be explained by the distribution of static pressure with various leans

in the control plane (Fig. 6.13). Isolines of static pressure in all cases are located almost vertically.

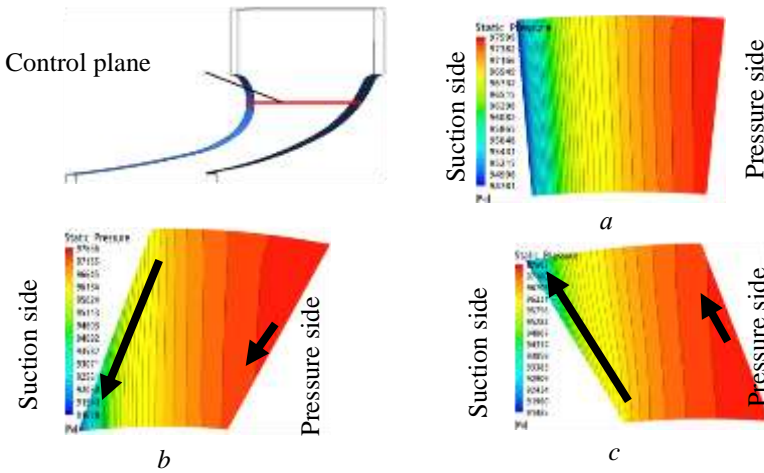


Figure 6.13 The contours of the static pressure at control plane at different leans: a – 0°; b – -30°; c – 30°.

In the cascade without lean (Fig. 6.13) the pressure gradient along the height of the blade is virtually absent, unlike the blades with lean (Fig. 6.13b and Fig. 6.13c). Negative lean (see Fig. 6.13b) leads to pressure gradient appearance along the height of the blades, directed from the periphery to the root and on the suction side of the blade it is more substantial than on its pressure side. Positive lean brings to appearance of the opposite to the direction of pressure gradient at the surface of the blade (Fig. 6.13c).

6.6 The Influence of Complex Tangential Lean on the Flow in Circumferential Turbine Cascade

Object of study and boundary conditions are identical to the turbine cascade, that described in the previous section, with the exception of the relative height

of the blade, which in this case amounted to $l/b = 0.714$. Complex lean was carried out according to 2-nd method without changing the stagger angle of the profile.

Using proposed algorithm (section 6.4) the optimal blade's shape of the specified turbine guide blade was found on the sixth step of the variation parameters range refinement.

All 56 configurations of turbine blades shape were counted.

To solve the same problem using genetic algorithm, probably, hundreds of calculations would have required. The Table 6.1 shows the best value of the varied parameters and the best value of target function for each of the optimization stages.

At the 1–5 stages optimization of minimum objective function fall on the border range of variation parameters, at that on 4-th phase the function is minimal on the right edge of the border of variation parameters range, while on 5-th phase the function is minimal on the left edge. As a result, after the 6-th phase the values of the optimal parameters became $Y_s = 0.77$ and $Y_h = 0.80$.

Table 6.1 History of optimization studies.

Stage	Initial	1	2	3	4	5	6
Range, Y_s	0	0,02–0,18	0,16–0,25	0,25–0,38	0,38–0,73	0,73–1,58	0,65–0,94
Range, Y_h	0	0,02–0,18	0,16–0,25	0,25–0,38	0,38–0,73	0,73–1,58	0,67–0,98
Y_s	0	0,18	0,25	0,38	0,73	0,73	0,77
Y_h	0	0,18	0,25	0,38	0,73	0,73	0,8
ζ_s , %	4,4010	4,3360	4,3025	4,2506	4,1688	4,1688	4,1687

Fig. 6.14 shows isolines of the objective function in the space of parameters Y_s and Y_h .

Lines of equal values of the objective function have incomplete shape due to the fact, that the obtained values of the function are distributed unevenly, and

most of them are situated in the neighborhood of line $Y_s = Y_h$. Dots on the Fig. 6.14 display the values of the parameters Y_s and Y_h on every stage of the optimization study. Comparison of Fig. 6.14 and Table 6.1 allows to see how the history of the changes Y_s and Y_h looks like.

Partial filling in by the calculation points of depicted area associated with large labour-intensive calculations and inability to evenly fill in the entire area. However, the carried out calculations are sufficient to argue that the domain of the minimum values of the target function was found. It is located near the center of the study area.

Fig. 6.14 shows that the objective function in the domain of minimum values has been changing slightly, which means that there is some freedom in choosing the optimal values of Y_s and Y_h .

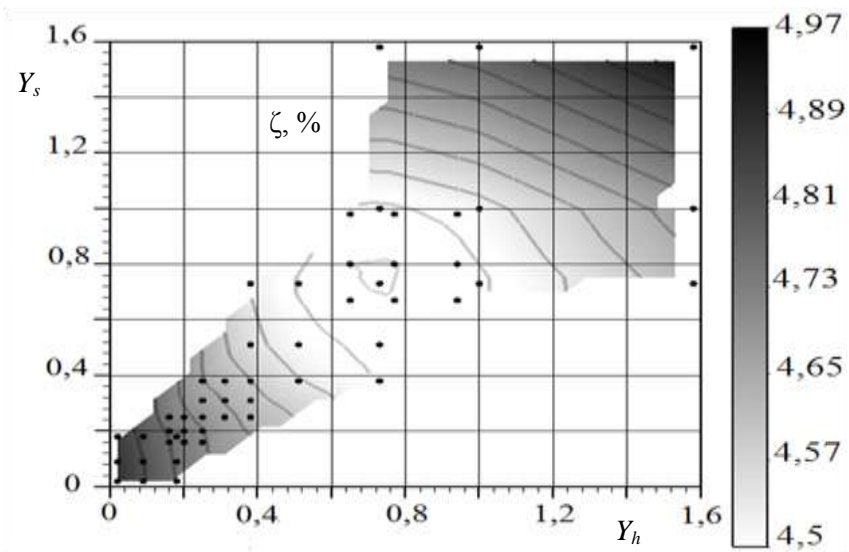


Figure 6.14 Isolines of integral losses.

Fig. 6.15 depicts the distribution of the losses coefficient of kinetic energy.

Analyzing these data, you can see that the peaks, characterizing horseshoe vortices in the optimal cascade, become less manifested and slightly have shifted in the direction of the flow center. Further confirmation of this is the distribution of the actual outlet flow angle in the optimal cascade (Fig. 6.16).

Indeed, looking at the optimized turbine blade (Fig. 6.17), we can see that in the bottom part of the blade the positive lean takes place and the negative lean has place at the top. It gave the possibility to obtain, predicted in the previous subsection, pressure distribution in the blade passage (Fig. 6.18) and on the suction side of the blade (Fig. 6.19), in other words, to combine the positive effects from simple leans, excluding the negative implications.

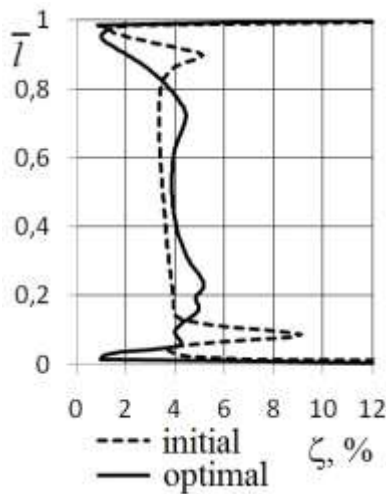


Figure 6.15 Distribution of the losses coefficient along the blade height.

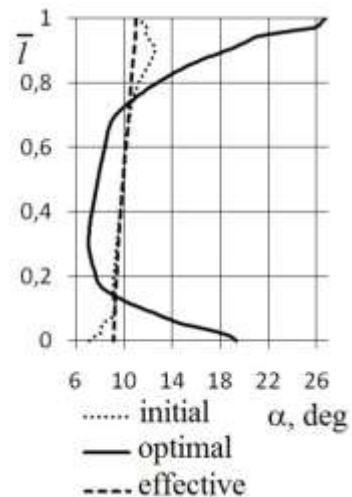


Figure 6.16 Distribution of the outlet flow angle along the blade height.

Some calculated characteristics of initial and optimized blade cascade has shown in the Table. 6.2. It is worth to note that mass flow rate and actual outlet flow angle has changed, and this changing is in the order of 10%. Changing of the outlet flow angle and, as a consequence, the mass flow rate is connected with changing of flow structure in the cascade and with reduced losses.

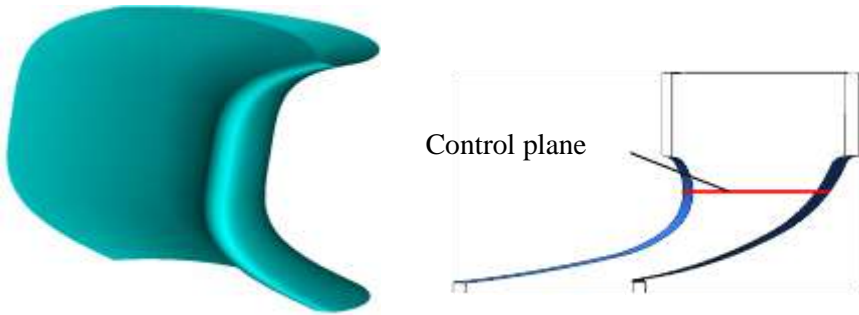


Figure 6.17 Optimal cascade.

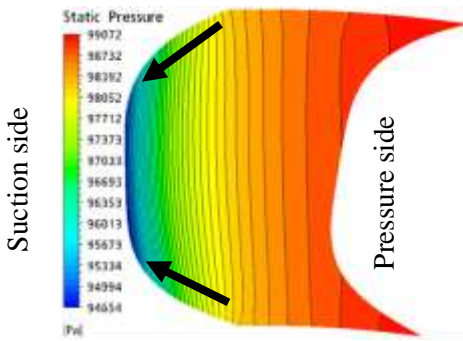


Figure 6.18 The contours of the static pressures at the control plane in the optimal cascade.

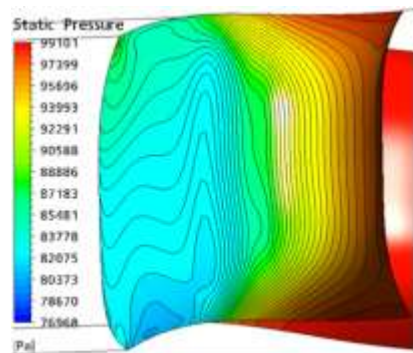


Figure 6.19 The contours of the static pressures at the low pressure side of the optimal cascade.

Table 6.2 Characteristics of the initial and optimal cascade.

Blade cascade	Mass flow rate, kg/s	α_1 , degree	ζ_{total} , %
Initial	0.9936	10.11	4.970
Optimal	1.0922	11.30	4.497

As a result, it can be stated that the proposed method gave the possibility to find the global minimum of the function, but the increase of the mass flow rate in the optimal cascade by almost 10% is unallowable.

So in further when conducting optimization this should be taken into account and the changing of the mass flow rate should be restricted by imposing an additional parameter of variation $\Delta\beta_s$.

6.7 Optimization with the Mass Flow Rate Preservation Through the Cascade

Review of research on the application of the complex tangential lean and its optimization, as well as conducted computational research has shown that using of complex lean gives the possibility to increase aerodynamic efficiency of turbine cascades. However, as previously noted, research on optimization of complex tangential lean with preserving mass flow rate through the cascade with high precision, currently we do not have. Using developed optimization approach it is possible to preserve in optimal cascade mass flow rate at the level of the initial cascade with a high accuracy.

Complex tangential lean reduces integral losses by reducing secondary losses. It is known, that with increasing l/b there is a reducing in the part of the secondary losses in integral losses and, accordingly, the benefit from optimization has to diminish.

Relative height criterion was taken not l/b , but the cascade's characteristic relation a/l , by analogy with the flows in the swivel tubes of rectangular cross-section.

Optimization problem is solved using two methods of stacking line parameterization. Research of the efficiency of the algorithm consists in attempts of optimization of turbine cascade at different $a/l = 0,16; 0,23; 0,44$ by changing of the blade height. It should be noted that for the blades with

$a/l \leq 0.16$ optimization, using both methods of stacking parameterization, no longer led to the reducing losses compared to the cascade without lean.

The size of the throat varies slightly due to the changing of stagger angle of the profile, which is associated with the preserving of the mass flow rate.

Special attention was given to the *FMM* accuracy, since it determines the validity of the results obtained with used optimization approach. Criterion of the accuracy is deviation of the values of the target function and the constraint function, which we obtain in *FMM* and in checking *CFD* calculation.

6.7.1 Optimization with Various a/l Using Method 1

The results of the optimization for $a/l = 0.44$

Taking into account the experience of previous studies, in Table 6.3 the ranges of parameters variation have shown. The correctness of their choice is confirmed by the fact that the optimal combination of varied parameters falls in this range already at the first step of the optimization.

Table 6.3 Ranges of variation of parameters optimization.

Parameter	min	max
Y_s	0.2	0.5
Y_h	0.6	0.9
$\Delta\beta_s$, degree	0	0.5

Then, a plan is created in accordance with the algorithm and relevant *CFD* calculations are produced (Table 6.4). The objective function – integral losses ζ , restriction function – mass flow rate through the calculation channel G .

A potential imperfection of the proposed optimization approach can be precision of the obtained *FMM*. Checking *CFD* calculation of optimal variant shows that the accuracy of the *FMM* is high because the objective function optimal values, projected by *FMM*, and restriction function with high enough

precision coincide with their values received as a result of *CFD* calculation (divergence in ζ is 0.005%, and in G – 0.017%). Differences of the mass flow rate in optimal and initial variant, based on the results of the *CFD* calculations, is 0.014%.

Table 6.4 Results of the optimization using method 1 for $a/l = 0.44$

Parameters	Y_s	Y_h	$\Delta\beta_s$, degree	ξ , %	G , kg/s
Initial	0	0	0	6.46483	0.288864
1	0.500	0.900	0.250	6.06853	0.290430
2	0.500	0.600	0.250	6.12689	0.286293
3	0.200	0.900	0.250	6.12155	0.288312
4	0.200	0.600	0.250	6.19087	0.284589
5	0.500	0.750	0.500	6.17293	0.280340
6	0.500	0.750	0	6.01586	0.296079
7	0.200	0.750	0.500	6.23117	0.278370
8	0.200	0.750	0	6.07275	0.294141
9	0.350	0.900	0.500	6.17547	0.281387
10	0.350	0.900	0	6.01665	0.297062
11	0.350	0.600	0.500	6.23770	0.277339
12	0.350	0.600	0	6.08898	0.293340
13	0.350	0.750	0.250	6.11509	0.287041
opt. <i>FMM</i>	0.495	0.799	0.249	6.08030	0.288855
opt. <i>CFD</i>	0.495	0.799	0.249	6.08063	0.288905

Turbine cascade, obtained as the result of optimization, is shown at Fig. 6.20. The losses of the optimal cascade were reduced on 0.384% in absolute value or on 6.31% in relative value.

The distribution of the coefficients of losses and the actual outlet angles along the height of the blades for the initial and the optimal variants are represented at Fig. 6.21 and 6.22 respectively. These figures show that increasing of the losses in optimal variant took place in the central part of the cascade along with

reduction of the losses at the end areas, while actual outlet angle, on contrary, decreased in the central part and at the end areas.



Figure 6.20 Optimal cascade obtained using method 1 for $a/l = 0.44$.

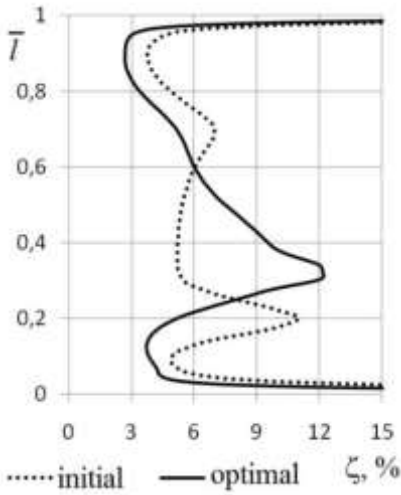


Figure 6.21 Distribution of the losses coefficient for $a/l = 0.44$.

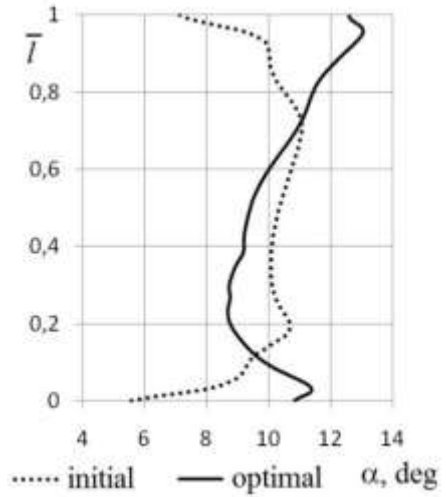


Figure 6.22 Distribution of the outlet flow angle for $a/l = 0.44$.

Table 6.5 Ranges of the variation of optimization parameters.

Parameter	min	max
Y_s	0.25	0.45
Y_h	-0.05	0.15
$\Delta\beta_s$, deg	-0.10	0.40

The results of the optimization for $a/l = 0.23$

Optimization results by method 1 at $a/l = 0.23$ were quite unexpected. Initial ranges of variation of parameters optimization were far from the final result. For this reason, the optimal variant was received only on the fifth stage of the optimization. Ranges of variation of parameters optimization of the fifth step are shown in the Table 6.5. Thus, to obtain the optimal variant in this case, 65 *CFD* calculations were required plus the calculation of initial variant and checking *CFD* calculation.

The appropriate calculation's plan for the fifth step with the results of determining the value of the target function, and restriction function listed in the Table 6.5.

Losses deviation between optimal variants for *FMM* and *CFD* made up 0.020% and the corresponding deviation of *G* in relative terms made up 0.006%. The mass flow rate was preserved with an accuracy of 0.004% in relative terms.

Table 6.6 Results of the optimization using method 1 for $a/l = 0.23$.

Parameters	Y_s	Y_h	$\Delta\beta_s$, degree	ξ , %	G , kg/s
Initial	0	0	0	5.45888	0.603025
1	0.450	0.15	0.15	5.32876	0.604827
2	0.450	-0.05	0.15	5.37593	0.599889
3	0.250	0.15	0.15	5.38874	0.598860
4	0.250	-0.05	0.15	5.44175	0.595029
5	0.450	0.05	0.40	5.45634	0.586522
6	0.450	0.05	-0.10	5.25013	0.617545
7	0.250	0.05	0.40	5.51989	0.581216
8	0.250	0.05	-0.10	5.31001	0.611905
9	0.350	0.15	0.40	5.46201	0.585955
10	0.350	0.15	-0.10	5.25297	0.616883
11	0.350	-0.05	0.40	5.50755	0.581701
12	0.350	-0.05	-0.10	5.30059	0.612414
13	0.350	0.05	0.15	5.38528	0.598818
opt. <i>FMM</i>	0.408	-0.0379	0.0816	5.35769	0.603015
opt. <i>CFD</i>	0.408	-0.0379	0.0816	5.35660	0.603049

Turbine cascade, obtained as the result of the optimization, is shown at Fig. 6.23. The losses of the optimal cascade were reduced on 0.102% in absolute value or on 1.89% in relative value.



Figure 6.23 Optimal cascade obtained using method 1 for $a/l = 0.23$.

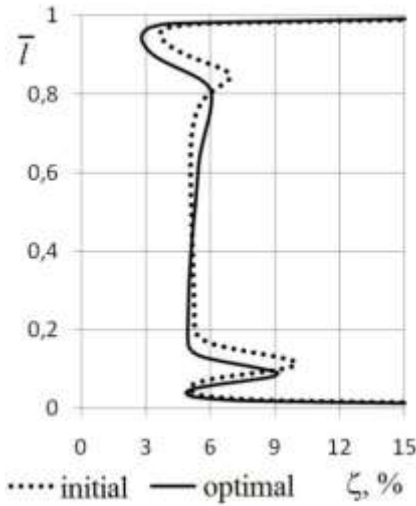


Figure 6.24 Distribution of the losses coefficient for $a/l = 0.23$.

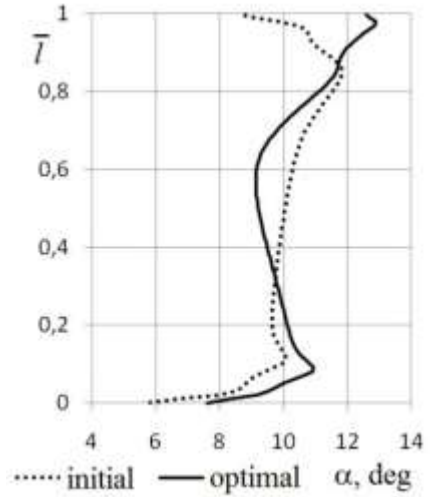


Figure 6.25 Distribution of the outlet flow angle for $a/l = 0.23$.

6.7.2 Optimization with Various a/l Using Method 2

The results of the optimization for $a/l = 0.44$

In this case were taken the ranges of parameters variation listed in the Table 6.7.

The solution was obtained in the first step of the optimization. The results of calculation using optimization method 2 have shown in the Table 6.8.

Table 6.7 Ranges of variation of parameters optimization.

Parameter	min	max
Y_s	0,2	0,5
Y_h	0,7	1
$\Delta\beta_s$, deg	0	0,5

In this case, losses deviation between optimal variants for *FMM* and *CFD* made up 0.006%, and the corresponding deviation of *G* in relative terms made up 0.017%. The mass flow rate was preserved with an accuracy of 0.017% in relative terms.

Table 6.8 Results of the optimization using method 2 for $a/l = 0.44$.

Parameters	Y_s	Y_h	$\Delta\beta_s$, degree	ξ , %	G , kg/s
Initial	0	0	0	6.46483	0.288864
1	0.5	1	0.25	6.22297	0.287388
2	0.5	0.7	0.25	6.24602	0.284416
3	0.2	1	0.25	6.27384	0.287651
4	0.2	0.7	0.25	6.28318	0.284258
5	0.5	0.85	0.5	6.29683	0.277681
6	0.5	0.85	0	6.15406	0.293667
7	0.2	0.85	0.5	6.36221	0.277942
8	0.2	0.85	0	6.19314	0.293665
9	0.35	1	0.5	6.33226	0.279469
10	0.35	1	0	6.16875	0.295172
11	0.35	0.7	0.5	6.34015	0.276185
12	0.35	0.7	0	6.18533	0.292074
13	0.35	0.85	0.25	6.24891	0.285655
opt. FMM	0.498	0.856	0.154	6.19839	0.288865
opt. CFD	0.498	0.856	0.154	6.19875	0.288914

Turbine cascade, obtained as the result of the optimization, is shown at Fig. 6.26. The losses of the optimal cascade were reduced on 0.266% in absolute value or on 4.20% in relative value.



Figure 6.26 Optimal cascade obtained using method 2 for $a/l = 0.44$.

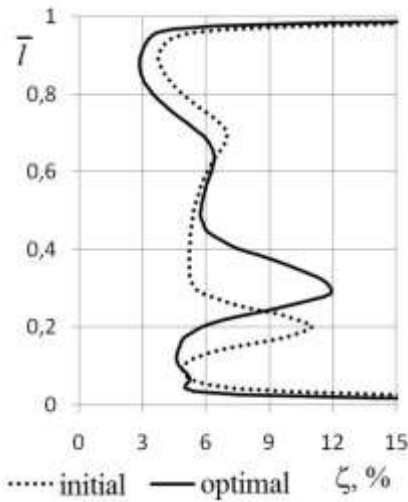


Figure 6.27 Distribution of the losses coefficient for $a/l = 0.44$.

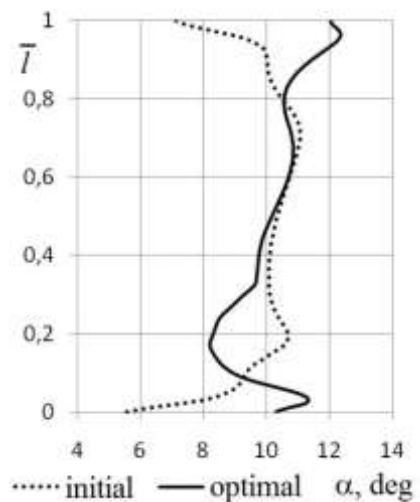


Figure 6.28 Distribution of the outlet flow angle for $a/l = 0.44$.

Comparing increasing of aerodynamic efficiency using methods 1 and 2, we can conclude that for this turbine cascade with $a/l = 0.44$ method 1 is more preferred because its use has significantly reduced integral losses.

The distribution of the coefficients of losses and the actual outlet angles along the height of the blades for the initial and the optimal variants are represented at Fig. 6.27 and 6.28 respectively. These figures show that increasing of the losses in optimal variant took place in the central part of the cascade along with

reduction of the losses at the end areas, while actual outlet angle, on contrary, decreased in the central part and at the end areas.

The results of the optimization for $a/l = 0.23$

Ranges of variation of parameters optimization are shown in the Table 6.5. In this case, the optimal variant was obtained at the first step of optimization.

Table 6.9 Ranges of variation of parameters optimization.

Parameter	min	max
Y_s	0.25	0.45
Y_h	0.40	0.60
$\Delta\beta_s$, deg	0	0.50

The plan of calculations with the results of determining the value of the objective function, and the restriction function listed in the Table 6.10.

In this case the losses deviation between optimal variants for *FMM* and *CFD* made up 0.032% and the corresponding deviation of *G* in relative terms made up 0.008%. The mass flow rate was preserved with an accuracy of 0.009% in relative terms.

Turbine cascade, received as the result of the optimization, is shown at Fig. 6.29. Losses in the new cascade made up 5.314% that on 0.145% in absolute value or on 2.69% in relative value is smaller than in the initial variant.

Application of the optimal complex lean by the method 2 when $a/l = 0.23$ resulted in a reduction of losses in end areas, but in the core of the flow losses remained almost unchanged. On contrary, actual outlet angle decreased in the central part of the cascade and increased in the end areas, the same as in the previous cases.

Thus, the optimization method 2 gave the possibility to reduce integral losses greater than method 1.

6.7.3 Reasons of Increasing the Efficiency of Optimized Cascades

Consider the flow in the initial cascade for $a/l=0.23$. Comparing the field of the total pressure at the value of $\bar{l} = 0.96$ and $\bar{l} = 0.5$ of the initial blade (Fig. 6.32), it can be seen that the thickness of the boundary layer in the similar areas much less at the height $\bar{l} = 0.96$ of the blade than in the core flow.

At the same time, the boundary layer thickness on its low-pressure side plays an essential role in the losses formation on the blade. This agrees well with the corresponding graphs of the losses coefficient distribution in height of the blade (see. Fig. 6.30).

Explanation of the reducing of boundary layer thickness in indicated areas at the periphery and the root can be given based on the analysis of the flow on the suction side of the blade (Fig. 6.33). On Fig. 6.33 line S marked the line of detachment of the channel vortex.

Table 6.10 Results of the optimization using method 2 for $a/l = 0.23$.

Parameters	Y_s	Y_h	$\Delta\beta_s$, degree	ξ , %	G , kg/s
Initial	0	0	0	5.45888	0.603025
1	0.450	0.600	0.250	5.29505	0.602551
2	0.450	0.400	0.250	5.35124	0.596915
3	0.250	0.600	0.250	5.32629	0.601706
4	0.250	0.400	0.250	5.38373	0.594765
5	0.450	0.500	0.500	5.41731	0.583745
6	0.450	0.500	0	5.22568	0.615261
7	0.250	0.500	0.500	5.45064	0.582208
8	0.250	0.500	0	5.25427	0.613547
9	0.350	0.600	0.500	5.41036	0.586293
10	0.350	0.600	0	5.21395	0.617685
11	0.350	0.400	0.500	5.46167	0.579785
12	0.350	0.400	0	5.26454	0.610895
13	0.350	0.500	0.250	5.33404	0.598298
opt. <i>FMM</i>	0.407	0.408	0.143	5.31201	0.603023
opt. <i>CFD</i>	0.407	0.408	0.143	5.31373	0.602973

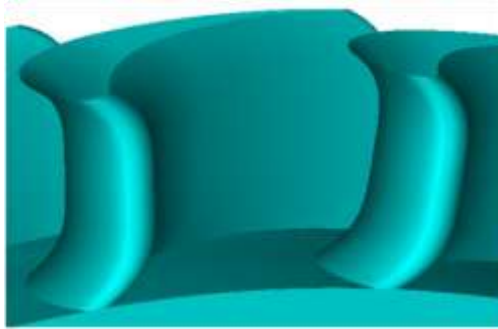


Figure 6.29 Optimal cascade obtained using method 2 for $a/l = 0.23$.

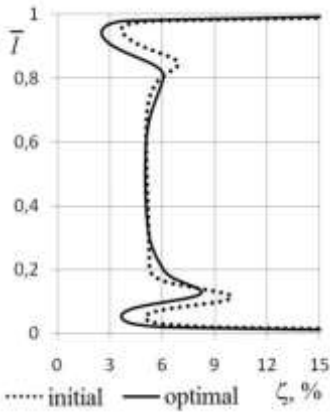


Figure 6.30 Distribution of the losses coefficient for $a/l = 0.23$.

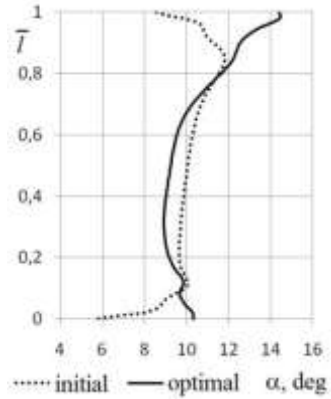


Figure 6.31 Distribution of the outlet flow angle for $a/l = 0.23$.

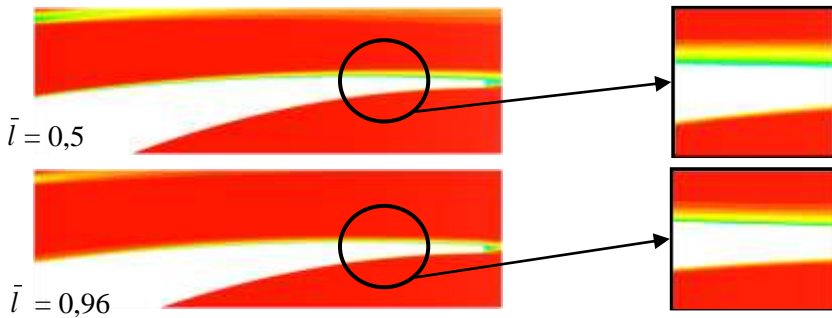


Figure 6.32 The field of the total pressure in the initial cascade.

It is the line of distinction of the two main border flows on the suction side of the blade:

- 1) flow along the blade from the leading edge to the trailing edge;
- 2) cross-over flow, that comes from the ends of the channel and penetrates, due to its inertia, on the blade (this flow is a part of the peripheral and root channel vortices) (Fig. 6.34).

Thus, on the suction side of the blades, there are areas with variously formed boundary layers. This explains the different thickness of the boundary layer in the appropriate places on the suction side of the blade.

As a result, the important conclusion can be formulated: the channel vortex leads to the formation on the suction side of the blade up to the line *S* of the boundary layer thickness less than the thickness of the boundary layer of the main flow around the blades. Thus the secondary flows have not only negative, but a positive effect, and properly distribution the stream structure can be used for creating optimal forms of turbine blades.

From the last considerations, it is possible to prove the reduction mechanism of aerodynamic losses for turbine cascade by applying optimal complex lean: the complex lean leads to the movement of the line *S* in the direction of the flow core and therefore to increasing the areas with smaller losses.

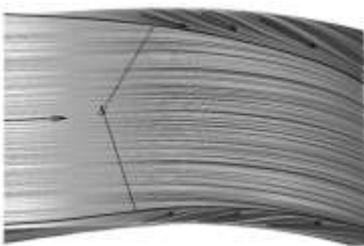


Figure 6.33 Stream lines on the suction side of the initial blade.

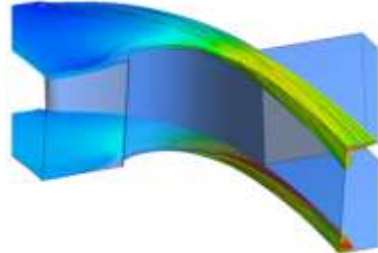


Figure 6.34 Stream lines of the secondary flow of the initial blade.

Displacement of the line S , when using complex tangential lean, takes place because of pressure gradient appearance on the suction side of the blade, which occurs when complex tangential lean is used. The result of this aerodynamic effect is certain offset of the saddle point from the pressure side of the blade to the suction side, therefore, to more earlier descent of the channel vortex from the end of the blade to the blade itself (Fig. 6.35). Descended on the blade, vortex, in turn, under the influence of pressure gradient slightly shifted on the blade toward the core of the flow, that leads to an increase of the part of the flow on the suction side of the blade with a smaller boundary layer than in the core of the flow.

As a result the proposed optimization algorithm made possible to find the optimum position of the line channel vortex detachment on the suction side of the blade by complex the lean optimization.

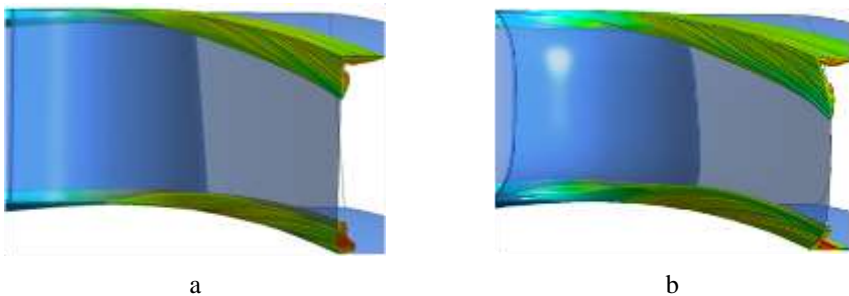


Figure 6.35 The move of the channel vortex on the suction side: a – initial cascade; b – optimal cascade using method 2.

